Too Many Junctions?

A Case Study of Multijunction Thin-Film Silicon Solar Cells

Si, Fai Tong; Isabella, Olindo; Zeman, Miro

DOI
10.1002/adsu.201700077

Publication date
2017

Document Version
Final published version

Published in
Advanced Sustainable Systems

Too Many Junctions? A Case Study of Multijunction Thin-Film Silicon Solar Cells

Fai Tong Si, Olindo Isabella, and Miro Zeman*

The benefit of two-terminal multijunction solar cells in regard to the number of junctions (subcells) is critically evaluated. The optical and electrical losses inherent in the construction of multijunction cells are analyzed using information from thin-film silicon photovoltaics as a representative case. Although the multijunction approach generally reduces the thermalization and nonabsorption losses, several types of losses rise with the number of subcells. Optical reflection and parasitic absorption are slightly increased by adding supporting layers and interfaces. The output voltages decline because of the tunnel recombination junctions, and more importantly of the illumination filtered and reduced by the top subcell(s). The loss mechanisms consume the potential gains in efficiency of multijunction cells. For thin-film silicon, the triple-junction is confirmed to be the best performing structure. More generally, only when each component subcell shows a high ratio between the output voltage and the bandgap of the absorber material, a multijunction cell with a large number of subcells can be beneficial. Finally, the high voltage and low current density of multijunction cells with a large number of subcells make them difficult to optimize and manufacture, vulnerable to any changes in the solar spectrum, and thus less practical for the ordinary terrestrial applications.

1. Introduction

The theoretical limit for the power conversion efficiency of photovoltaic cells is 33.1%[1] in the case of a single p–n junction under unconcentrated sunlight—widely known as the Shockley–Queisser limit.[2] Such efficiency can be surpassed by loosing some of the restrictions which define the limit. First, when the incident irradiance is increased by a concentrator, the ratio of photocurrent to dark current of the solar cell is increased, leading to higher open-circuit voltage (V_{OC}) and fill factor (FF). Second, by stacking up multiple p–n or p–i–n junctions (each of which is referred to a subcell) using absorber materials with different energy bandgaps, multijunction solar cells can reduce the thermalization and nonabsorption losses, meaning less spectral mismatch and a better spectral utilization. The theoretical efficiency limit of the solar cell comprising infinite number of component subcells is 68.2% without concentration and 86.8% with concentration.[3] In practice, the III-V photovoltaic technology represents a very successful demonstration of both strategies.[4,5] Within this category, the benefit of multijunction concept is apparent as the record efficiency of concentrator photovoltaic cells is 29.3% for the single-junction, and grows to 34.2%, 44.4%, and 46.0% for the monolithic two-terminal double-, triple-, and quadruple-junction cells, respectively.[6–9]

Multijunction solar cells can be made with two or more external electrical contacts (terminals). The components in a monolithic two-terminal device are considered to be in series connection. Therefore, the output current of a two-terminal device is constrained by the component which supplies the least photocurrent. Despite the limitation, two-terminal multijunction cells are much more feasible to design and manufacture than the ones with more terminals, thus more practical for applications. This type of two-terminal devices is the subject of this paper. For simplicity, we refer two-terminal multijunction solar cells to as multijunction solar cells, without further specification.

While the multijunction III-V solar cells mark the highest achieved power conversion efficiency of photovoltaic cells to date, the multijunction concept has been explored and developed in many other photovoltaic technologies as well. Besides the reduction of losses originating from spectral mismatch, the multijunction concept offers some additional benefits to the thin-film photovoltaics. The effective absorption is split into a few separate layers in different subcells, meaning that each layer can be made thinner for the same total absorption. Such thickness reduction improves the electrical performance when the carrier transportation in the material is a limiting factor. Moreover, the division of photocurrent implies less resistive losses over the electrical interconnections. The thin-film silicon solar cell has a long history of developing multijunction solutions to make use of these advantages. The efficiency improvement by additional subcells has been shown up to the triple-junction configuration.[10–17] In organic photovoltaics, the absorber materials have rather narrow absorption spectra.

F. T. Si, Dr. O. Isabella, Prof. M. Zeman
Photovoltaic Materials and Devices Laboratory
Delft University of Technology
Mekelweg 4, Delft, 2628 CD, The Netherlands
E-mail: f.t.si@tudelft.nl

DOI: 10.1002/adsu.201700077

Tandem (double-junction) devices with different materials can help to cover a broader part of the solar spectrum, thus have become the subject of active researches for over two decades.[18–20] In general, the multijunction concept attracts more research efforts whenever a photovoltaic technology becomes relatively mature and approaches its practical performance limit of the single-junction. Moreover, hybrid tandem solar cells integrating different photovoltaic technologies have drawn more and more attention over the past years in the pursuit of higher efficiencies. To name a few notable examples, the perovskite/crystalline silicon tandem,[21–24] perovskite/copper indium gallium selenide (CIGS) tandem[25] and hydrogenated amorphous silicon (a-Si:H)/organic double- and triple-junction solar cells[26] have all demonstrated the potential of exceeding the efficiency of the component single-junction cells. When the absolute efficiency is the main concern, making multijunction solar cells is the inevitable trend.

How many junctions (subcells) are too many? Ideally, the more subcells are properly integrated in a device, the better performance the device can provide. The gain from putting on one more additional subcell, however, becomes less with the increased number of subcells. Practically, there is a certain point that $N + 1$-junction cells can unlikely outperform N-junction cells in spite of the best engineering efforts. The efficiency improvement has not been achieved beyond the 5-junction configuration in case of the highly mature and extensively optimized III-V photovoltaics.[8,9,27] While the restriction of developing III-V solar cells with more subcells largely lies in the search of material systems with suitable bandgaps and achievable by compatible fabrication techniques, there are other limiting mechanisms which can play a bigger role in different multijunction photovoltaic technologies. Optical and electrical losses can occur in the sophisticated device structures, beside the impact of filtered sunlight on the optoelectrical response of the subcells. In these respects, the thin-film silicon photovoltaics is very interesting for studying the multijunction concept. The lesser transport properties of electrical carriers and the weak absorption coefficient near the band edge of the materials pose great challenges to the design and optimization of the device structures. Up to now, the highest initial efficiencies of thin-film silicon solar cells reported in literature are 11.8%,[10] 14.8%,[12] 16.3%,[14] and 15.0%[28] for the single-, double-, triple-, and quadruple-junction configurations, respectively. Remarkably, multijunction thin-film silicon solar cells have achieved high efficiencies with some very complicated structures. On the other hand, it is still under question whether the record held by the triple-junction can eventually be broken by a structure comprising even more subcells.

In this work, we evaluate the effects of the increased number of subcells on the performance of multijunction solar cells. By carefully examining the optical and optoelectrical losses which originate from the multijunction approach, the realistic benefit of making multijunction cells is studied.

2. Device Structures and Outline

Five different structures of multijunction thin-film silicon solar cells with up to four subcells were studied. In the order of decreasing bandgap, the absorber materials include (W)a-Si:H (wide-gap hydrogenated amorphous silicon), (N)a-Si:H (narrow-gap a-Si:H), a-SiGe$_x$:H (hydrogenated amorphous silicon germanium), and nc-Si:H (hydrogenated nanocrystalline silicon), providing a great variety of materials with different spectral sensitivity. The cell structures, identified by the absorber materials, are shown in **Table 1**. They are the single-junction nc-Si:H cell (S), the conventional double-junction a-Si:H/nc-Si:H cell (D), the triple-junction cell with nc-Si:H (TS) or a-SiGe$_x$:H (TG) in the middle subcell, and the quadruple-junction cell with nc-Si:H (QS) or a-SiGe$_x$:H (QG) in the third subcell. These structures are chosen for comparison because of their reported use in literature[13,14,29,30] and the different arrangements of the absorber bandgap. This is not an exhaustive list of all reported multijunction configurations,[28,29,31] but sufficiently representative for the purpose of this study. Configuration D, TG, and QG provide descending bandgaps of absorber materials along the direction of light incidence, therefore they should offer reasonable spectral utilization, fulfilling the goal of the multijunction concept. On the other hand, configuration TS and QS were widely used in literature because the emphasized use of nc-Si:H mitigates the light-induced degradation of the whole device.

Table 1. Material configurations of the studied single and multijunction solar cells. The structures are the single-junction (S), double-junction (D), triple-junction with either nc-Si:H (TS) or a-SiGe$_x$:H (TG), and quadruple-junction with either nc-Si:H (QS) or a-SiGe$_x$:H (QG). (W)a-Si:H and (N)a-Si:H are the wide-gap and narrow-gap a-Si:H, respectively.

Subcell	S	D	TS	TG	QS	QG
1st	nc-Si:H	(N)a-Si:H	(W)a-Si:H	(W)a-Si:H	(W)a-Si:H	(W)a-Si:H
2nd	–	nc-Si:H	nc-Si:H	a-SiGe$_x$:H	(N)a-Si:H	(N)a-Si:H
3rd	–	–	nc-Si:H	nc-Si:H	nc-Si:H	a-SiGe$_x$:H
4th	–	–	–	–	nc-Si:H	nc-Si:H

The different multijunction structures are compared by their photovoltaic performance. First of all, Section 3 derives the potential efficiencies of the studied solar cells from the properties of high-quality single-junction cells and a set of optimistic assumptions. Starting from this baseline, several loss mechanisms are investigated in the following sections to approach a more realistic estimation of the efficiencies. Section 4 uses optical modeling to inspect the spectral response of the structures and study how the number of subcells influences the absorption and reflection of the solar cells. The way how a multijunction cell is formed determines its output voltage. Concerning the voltages, the effect of tunnel recombination junctions (TRJs) is discussed in Section 5 while the effect of different irradiance experienced by each subcell is discussed in Section 6. Material properties define what device structures are feasible, and Section 7 shows how the restriction on absorber thickness changes the attainable efficiencies. Section 8 comments on what should be considered in the pursuit of higher efficiencies by multijunction solar cells. Last but not least, the impact of current matching/mismatch on the performance of multijunction solar cells, especially how the cells with different numbers of subcells react to the variation in solar spectrum, is examined in Section 9.

Table 2. V_{OC} and J_{SC} of single-junction solar cells under AM1.5G (1 sun) illumination.

	$V_{OC-1sun}$ [V]	$J_{SC-1sun}$ [mA cm^{-2}]	Ref.
(W)a-Si:H	1.024	9.73	[14]
(N)a-Si:H	0.901	16.55	[32]
a-SiGe$_x$:H	0.764	18.87	[14]
nc-Si:H	0.552	25.60	[12]

3. Lossless Estimation

To start the comparison, the efficiency potential of these structures is estimated by neglecting many sources of power losses. Several optimistic assumptions are used for this estimation. First, the V_{OC} of the multijunction cell is the simple arithmetic sum of the V_{OC} of the component single-junction cells, which were individually made and measured under AM1.5G solar spectrum. No additional voltage losses are present in the formation of the multijunction. The external parameters of some best single-junction cells reported in literature[12,14,32] are shown in **Table 2**, and their V_{OC} is used in the estimation. Second, the photocurrent is perfectly divided among the component subcells, and the total photocurrent density is 32.9 mA cm^{-2}, the highest reported short-circuit current density (J_{SC}) for single-junction nc-Si:H solar cells.[33] This assumption represents the optimal light trapping and current matching, as well as the minimal optical losses. Third, the *FF* is fixed at a high value of 77% which might be realized by exceptional device optimization.[14] Following these assumptions, the external parameters of the studied structures are derived and shown in **Table 3**.

Based on the parameters reported in literature and with some optimistic assumptions, the performance shown in Table 3 serves as the upper limit of these structures where most optical and electrical losses related to multijunction cells are neglected. In such optimistic scenario, the implied efficiency (η) highly depends on the choice of materials. The use of the same material (nc-Si:H) in two subcells results in the lower efficiencies of structure TS and QS, compared to their counterparts in which all absorber materials are different. The triple-junction structure TS even performs worse than the double-junction structure D in this calculation. As expected, efficiency improvements are suggested between structures S, D, TG, and QG when the number of subcells increases and different absorber materials with proper bandgaps are used.

Table 3. External parameters of thin-film silicon solar cells estimated by optimistic assumptions.

	S	D	TS	TG	QS	QG
V_{OC} [V]	0.552	1.453	2.128	2.340	3.029	3.241
J_{SC} [mA cm^{-2}]	32.9[33]	16.45	10.97	10.97	8.23	8.23
FF [%]	77.0[14]					
η [%]	13.98	18.40	17.97	19.76	19.18	20.52

4. Optical Analysis

When the number of subcells increases, the increase in the total absorber thickness can possibly enhance the effective absorption of the device. Nevertheless, the parasitic absorption and reflection may also increase because of the additional supporting layers and interfaces, leading to extra optical losses. (Here supporting layers include all layers which are not an absorber layer.) The quantitative examination of the absorptance and reflectance is desired for studying the effects of multijunction structures on the optical response of the devices. Optical modeling and simulations provide a powerful tool to reveal such internal quantities which can hardly be accessed by measurements.

The model GenPro4,[34] which is suitable to concurrently model different optical regimes from refraction to diffraction, was used to simulate the optical response in the studied structures. The information of the layers and scattering interfaces define the structure in the optical model. The refractive index and absorption coefficient (or extinction coefficient) of the materials were either measured internally by spectroscopic ellipsometry or adopted from literature. Such optical constants of all materials used in the studied structures are shown in **Figure 1**. In respect of the light scattering, the modulated surface texture (MST) was proved an effective light scatterer and in-coupler in a broad spectral range.[12,35,36] Together with highly transparent supporting layers and a silver back reflector, the MST was applied in the simulations of all studied structures to examine the optical performance within state-of-the-art light trapping scheme.[37] In the model, the MST was realized by assigning a refractive scattering interface between the microtextured glass and the transparent conductive oxide (TCO), and a diffractive scattering interface on top of nonintentionally doped ZnO[38]—mimicking how the MST is fabricated experimentally.[12] The thicknesses of the doped layers and other supporting layers were fixed in the simulated structures at the typical values used in actual devices. To enable a relevant comparison between the studied structures, the thicknesses of the absorber layers were optimized per case. In all structures, the thickness of absorber layer in the bottommost subcell, which is nc-Si:H, was predetermined at 3500 nm. Such thickness suggests a relatively thick nc-Si:H layer for the absorption of near-infrared light while being able to support a decent carrier transportation. The thicknesses of other absorber layers were iteratively adjusted in the model until the current-matched condition, that the implied photocurrent densities (J_{ph}) of all absorber layers within a structure are equal, is fulfilled. This matched J_{ph} can be approximated as the J_{SC} of the multijunction cell. As an extensive example, the information used in the simulation of structure QG is given in **Table 4**.

The simulated optical response of the studied structures is shown in **Figure 2**. The simulation calculates the spectral absorptance of each layer and the total reflectance of a given structure. Figure 2a demonstrates the absorption in each layer of the single-junction structure S with respect to the photon flux density of AM1.5G illumination. For better clarity, Figure 2b–f only plot the absorptance of the absorber layers in the multijunction structures, together with the respective total

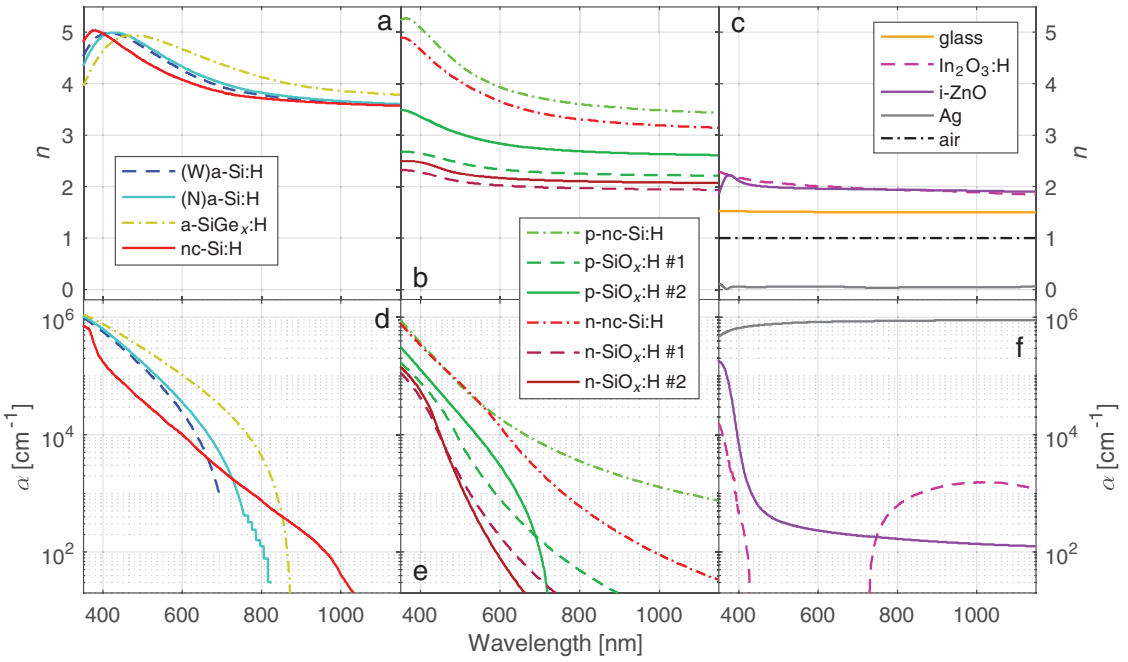

Figure 1. The wavelength-dependent refractive index (n) and absorption coefficient (α) of the a,d) absorber materials, b,e) doped materials, and c,f) other supporting materials, used in the studied multijunction solar cells.

absorption derived from $1 - R$, where R is the total reflectance. In structures TG and QG, there is less spectral overlap between the two bottom subcells than there is in structures TS and QS. This suggests a better spectral utilization by the absorber configurations in TG and QG.

Table 4. The simulated structure of QG. p-SiO$_x$:H #1 and n-SiO$_x$:H #1 are with higher oxygen content, larger bandgap, and lower refractive index, compared to p-SiO$_x$:H #2 and n-SiO$_x$:H #2. In spite of its absorptive nature, the thin p-nc-Si:H layer was used in the device to mitigate the transport barrier between the TCO and the p-layer.[39] The thickness of nc-Si:H absorber, t_4, was fixed at 3500 nm in the simulation.

Material	Thickness [nm]
Air	infinite
Glass	7×10^5
In$_2$O$_3$:H	140
ZnO	1000
p-nc-Si:H	4
p-SiO$_x$:H #1	8
(W)a-Si:H	t_1
n-SiO$_x$:H #1	30
p-SiO$_x$:H #1	8
(N)a-Si:H	t_2
n-SiO$_x$:H #1	30
p-SiO$_x$:H #2	16
a-SiGe$_x$:H	t_3
n-SiO$_x$:H #2	30
p-SiO$_x$:H #2	12
nc-Si:H	t_4
n-SiO$_x$:H #2	60
Ag	Infinite

4.1. Spectral Overlap

A spectral overlap between the absorption spectra of two subcells means that photons with a wavelength within the overlapping region can generate carriers in more than one subcell. When the absorber materials of the spectrally overlapping subcells have different bandgaps, some of the high-energy photons which can potentially be used by the wide-gap material are absorbed and converted in the narrow-gap material, leading to a lower generated voltage and more thermalization losses. While the spectral overlap cannot be eliminated due to the absorption properties of the materials, some unnecessary losses caused by the design of device structure should be avoided. For example, in the case of structure QS or QG, the topmost absorber layer is made too thin that it does not fully utilize the effective spectrum of the material so some of the high-energy photons are absorbed in the subsequent subcells. The insufficiently thick absorber layers therefore induce extra thermalization losses. Such designs are less ideal and should be avoided. Furthermore, the concern of spectral overlap suggests that in a multijunction solar cell, the use of absorber materials with indirect bandgap and lesser absorption capability should be limited. These materials, such as nc-Si:H or nc-SiGe$_x$:H, should only be used in one subcell at most. When used, it should be placed only in the bottommost subcell. Otherwise, the use of these materials in two or more subcells, or in a nonbottommost subcell, will lead to significant spectral overlap and thermalization losses.

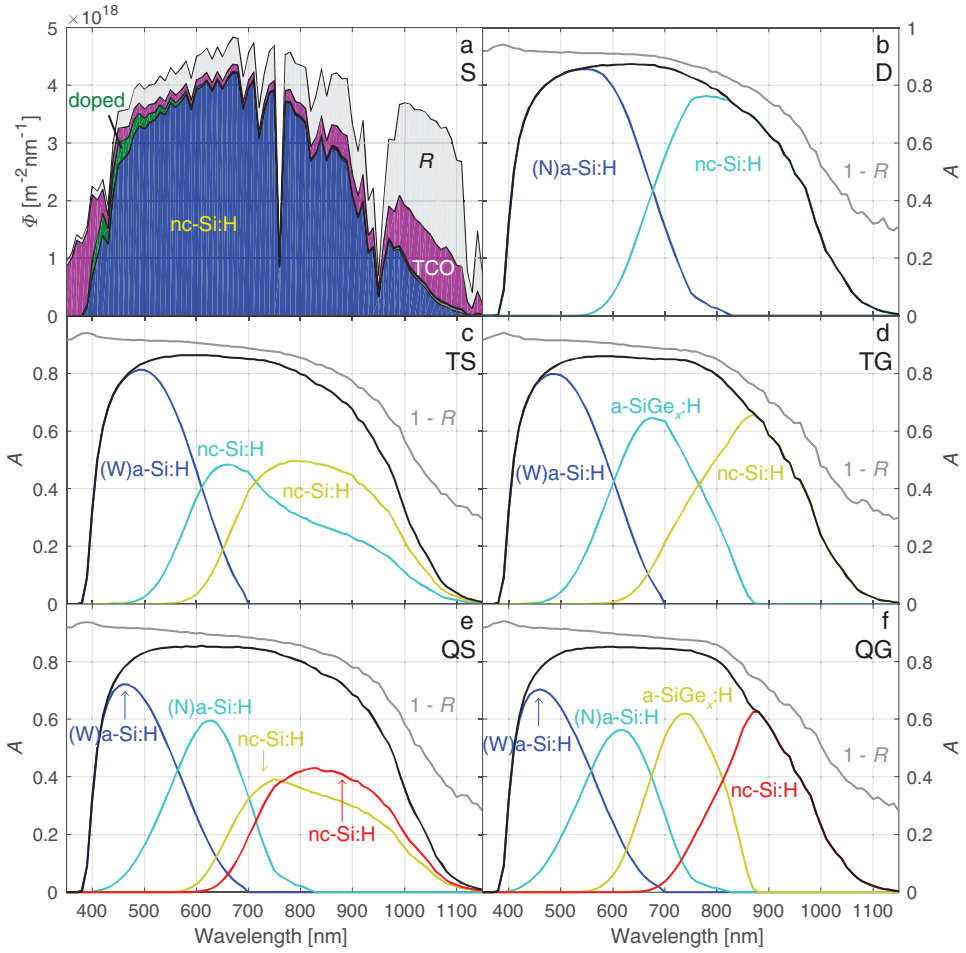

Figure 2. Simulated optical response of the studied structures. a) The absorbed and reflected photon flux density of structure S, with respect to AM1.5G illumination. b–f) The effective absorptance and $1 - R$ in structure b) D, c) TS, d) TG, e) QS, and f) QG. The solid black lines show the sum of effective absorptance from all absorber layers.

4.2. Parasitic Absorption

The absorption in the supporting layers including the TCO and the doped layers does not result in collectable photocurrent in the external circuit, thus is regarded as parasitic absorption and a major cause of optical losses. Intuitively, one may expect more parasitic absorption in the structure with more subcells taking the extra intermediate layers into account. This speculation was examined using the data available from the optical simulations.

Figure 3 shows the absorption in different layers in the form of equivalent J_{ph} under AM1.5G spectrum. The J_{ph} was calculated by Equation (1)

$$J_{ph} = e\int_{300\,nm}^{1200\,nm} A(\lambda)\Phi(\lambda)\mathrm{d}\lambda \quad (1)$$

where e is the elementary charge, $A(\lambda)$ is the wavelength-dependent absorptance of a layer or the total reflectance, $\Phi(\lambda)$ is the spectral photon flux density of AM1.5G spectrum. In Figure 3a, all absorption and reflection in a structure are included, so the sum is always 46.48 mA cm^{-2}, which accounts for the photons available in the wavelength range from 300 to 1200 nm. The parasitic absorption in the TCO layers is comparable throughout the studied structures. Interestingly, the total effective absorption increases in the order of S, D, TS, to QS, but decreases in the order of D, TG, to QG. The parasitic absorption in the doped layers is individually presented in Figure 3b. The bars in the darkest green indicate the contribution of the p-layers in the topmost subcells. Then, the bars in lighter green represent the absorption in the subsequent doped layers which also act as the TRJ. Noticeably, the parasitic absorption in the doped layers is dominated by the p-layer of the topmost subcell, where the majority of visible light is absorbed. The subsequent doped layers are mostly transparent to the residual photons which have lower energy. The absorption in the subsequent doped layers becomes apparent with the increased number of subcells, as the absorption spectra of the topmost subcells become narrower and more reddish photons can arrive at the subsequent layers. Especially, to match the photocurrent in the quadruple-junction structures, the topmost absorber should only utilize the bluest part of the spectrum, making the leftover susceptible to parasitic absorption. Quantitatively speaking, the transparency of the doped materials plays a bigger role than the device structure. A less transparent

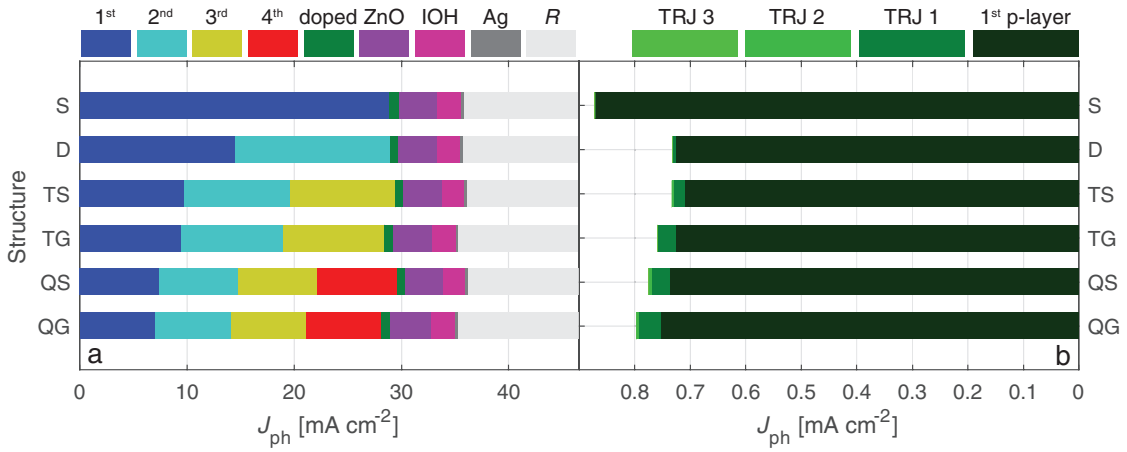

Figure 3. a) The absorption in different layers and the total reflection of the studied structures, equivalent to photocurrent density J_{ph} under AM1.5G spectrum. IOH stands for In_2O_3:H, the use of which is indicated in Table 4. b) The parasitic absorption in the doped layers. TRJ 1 is the TRJ between the first and second subcells, etc.

p-layer used in structure S is responsible for the considerably larger parasitic absorption. Even in the subsequent layers, an insertion of a less transparent 4-nm n-type nc-Si:H layer between the first and second subcells of the structure QG can increase the parasitic absorption by 0.088 mA cm^{-2} equivalent, which is a relative increase of 11.1%. To sum up, in the consideration of parasitic absorption, device structures with less subcells are favorable, on the basis of using highly transparent supporting materials.

4.3. Reflection Losses

Reflection occurs when light impinges upon an interface between two media. In solar cells, beside the primary reflection at the surface which directly decides the amount of photons entering the cell, the intermediate reflection between the interfaces inside the cell can also influence the optical response, both positively and negatively. With the information extracted from the simulations, **Figure 4**a illustrates how the reflection develops along the structure of solar cell QG and results in the total reflectance measurable from the surface. The x-axis shows the depth (not in scale) related to the cell structure and the materials are indicated. The profile drawn in a solid line sketches the change of refractive index n of the materials along the depth. The overlaying stem plot shows the accumulated reflection up to a certain interface, in the form of equivalent photocurrent (J_R) under AM1.5G spectrum. The primary reflection at air/glass interface is worth 1.90 mA cm^{-2} as indicated. Before the light enters the topmost (1st) subcell, the refractive index increases stepwise from that of the air to the first absorber. The small steps in n offer an antireflection effect, but the abrupt increase in n at the first subcell still causes noticeable intermediate reflection. The highly transparent doped hydrogenated silicon oxide (SiO_x:H) materials have relatively large bandgap and low refractive index. The contrast in n between the absorber and doped materials is depicted by the profile, which raises the accumulated reflection whenever a subsequent subcell is encountered. In the end, the remaining photons which are not absorbed are reflected back by the metal (Ag) reflector.

The intermediate reflection occurring at the subsequent subcells can be a source of optical losses. In Figure 4b, the spectral photon flux density of the reflection supplemented by different interfaces in structure QG, with response to AM1.5G incident spectrum, are stacked to show how each interface builds up the accumulated reflection. It should be pointed out that the intermediate reflection at the subsequent subcells is mostly constituted of low-energy photons, which can be utilized by the bottom subcells but not the top ones. To clarify this behavior, it can be seen in Figure 4b that the intermediate reflection from the 1st, 2nd, 3rd, and 4th subcell starts from the wavelength around 400, 500, 650, and 750 nm, respectively. These reflected photons then escape the solar cell and are lost.

The different components of the accumulated reflection from the studied structures are compared in Figure 4c. It is clear that the more subcells there are in a structure, the more intermediate reflection occurs and the less infrared light can arrive at the bottommost absorber layer. It explains the observation in Figure 3a that the effective absorption decreases with the increased number of subcells in the group in which a-SiGe$_x$:H is used (D > TG > QG). In the group of S, D, TS and QS, the impact of reflection losses is offset by the absorption of the thick nc-Si:H layer in the penultimate subcell of structures TS and QS.

Having considered the effects of parasitic absorption and intermediate reflection, it is suggested from the optical point of view that the multijunction solar cells with more subcells are more susceptible to parasitic losses, and thus also require more delicate design and better engineering to overcome the added hurdles.

5. Tunnel Recombination Junctions

As the subcells in two-terminal multijunction solar cells are connected in series, the electrons/holes generated in a subcell need to recombine with the holes/electrons from the neigh-

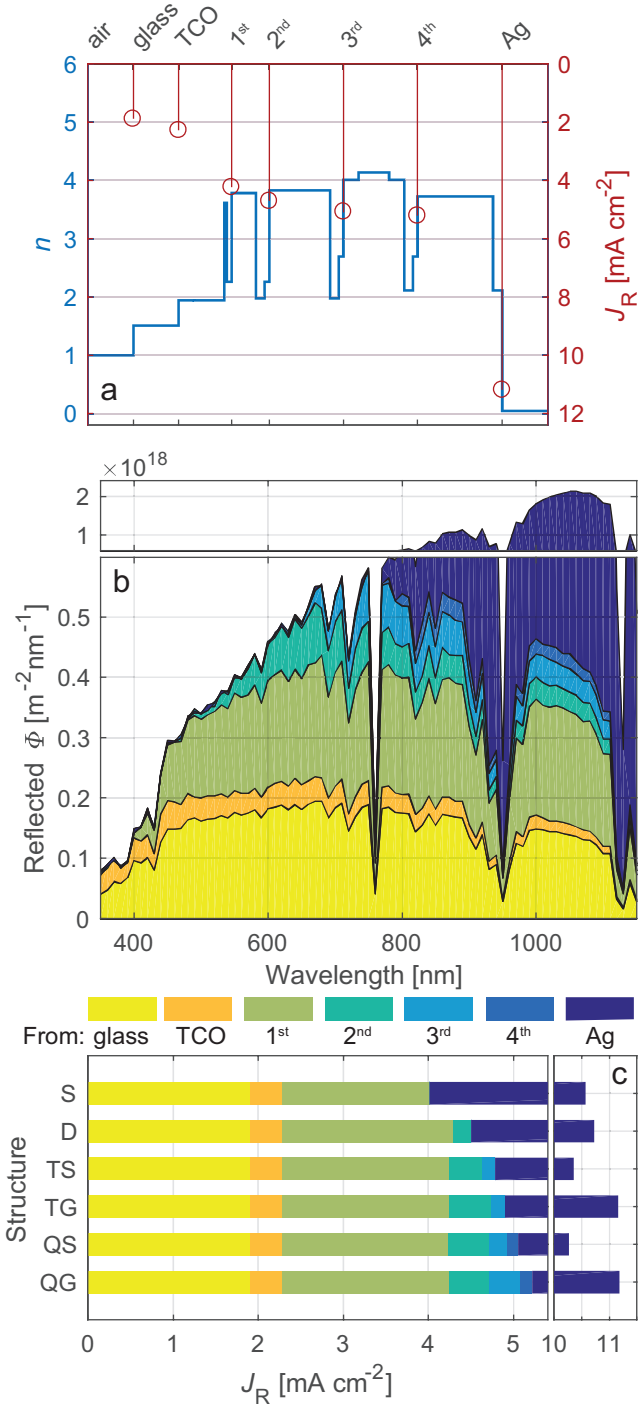

Figure 4. Reflection accumulated from different interfaces in multijunction solar cells. a) Left-axis: The profile of refractive index n against the depth in the cell, and right-axis: the equivalent photocurrent J_R of the accumulated reflection up to certain interfaces, in the structure QG. b) Spectral photon flux density of the accumulated reflection up to certain interfaces in the structure QG. c) J_R of the studied structures, dissected with the contributions of different interfaces.

boring subcell, taking place near the border between the two subcells. Such process is facilitated by the tunnel recombination junction between the subcells, which can comprise the doped layers between the two absorber layers, possibly with other functional layer(s). When the recombination is not efficient enough, the accumulated carriers lead to a potential barrier and thus a drop in the output voltage of the solar cell.

Table 5. Effects of voltage losses due to TRJs and filtered illumination. The photocurrent densities used for the calculations are derived from the optical simulations. The FF is fixed at 77%. a) The baseline performance without voltage losses (Lossless), meaning that the V_{OC} is the sum of the component V_{OC} shown in Table 2. Then, either the effect of b) TRJs or c) filtered illumination is considered solely. d) Both sources of losses are taken into account. In the calculation, $T = 298.15$ K is used.

		D	TS	TG	QS	QG
	$J_{ph\text{-}tot}$ [mA cm^{-2}]	28.92	29.41	28.45	29.56	28.14
	J_{SC} [mA cm^{-2}]	14.46	9.80	9.48	7.39	7.03
a) Lossless	V_{OC} [V]	1.453	2.128	2.340	3.029	3.241
	η [%]	16.18	16.07	17.09	17.24	17.55
b) TRJ	ΔV_{OC} [mV]	−15	−30	−30	−45	−45
	V_{OC} [V]	1.438	2.098	2.310	2.984	3.196
	$\Delta\eta$ [%]	−0.17	−0.23	−0.22	−0.26	−0.24
	η [%]	16.01	15.84	16.87	16.98	17.31
c) Filtered	ΔV_{OC} [mV]	−27.2	−73.7	−65.8	−137.4	−133.3
	V_{OC} [V]	1.426	2.054	2.274	2.892	3.107
	$\Delta\eta$ [%]	−0.30	−0.56	−0.48	−0.78	−0.72
	η [%]	15.87	15.51	16.61	16.45	16.83
d) Combined	V_{OC} [V]	1.411	2.024	2.244	2.847	3.062
	η [%]	15.71	15.28	16.39	16.20	16.59

The influence of TRJs on the studied structures of multijunction thin-film silicon solar cells was assessed. In **Table 5**, the total effective $J_{ph\text{-}tot}$ obtained in the optical simulations was listed to determine the J_{SC} used in this estimation. Together with the lossless V_{OC} given in Table 3 and a fixed FF of 77%, the derived efficiency η serves as the baseline in the analysis of the electrical losses. With J_{SC} adjusted by the simulations yet other parameters unchanged, the baseline efficiencies follow the same trend as the ones shown in Table 3. As a simplistic assumption, the loss of V_{OC} at a TRJ is assumed at a universal value of −15 mV per TRJ regardless of the actual structure. The value was chosen to represent a well-engineered TRJ with a minute amount of voltage drop.[14,28,30,40] The resulted voltage and efficiency are shown in Table 5. Although the loss in voltage linearly increases with the number of TRJ, the loss in efficiency is not as severe when the number of subcells becomes large. In terms of the efficiency loss ($\Delta\eta$) caused by TRJs, the difference between the triple-junction and quadruple-junction structures in the same group is merely in the range of 10% relative.

The inconsistency between the losses in voltage and in efficiency can be explained by the change in current density. For a multijunction solar cells consisting of N subcells and $N-1$ TRJs, the loss in efficiency $\Delta\eta$ caused by TRJs is

$$\Delta\eta = (N-1)\cdot\Delta V_{TRJ}\cdot\frac{J_{ph-tot}}{N}\cdot FF/I \quad (2)$$

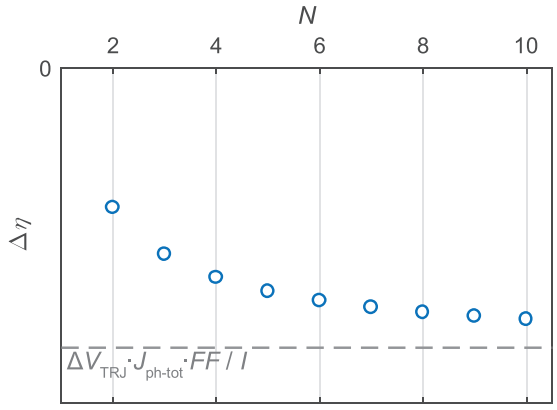

Figure 5. The loss in efficiency $\Delta\eta$ of multijunction solar cells caused by the voltage drop at the TRJs. The magnitude of $\Delta\eta$ increases and saturates with the number of subcells N.

assuming the loss in V_{OC} caused by each TRJ is a constant ΔV_{TRJ}, the total photocurrent density $J_{ph\text{-}tot}$ is unchanged (under incident irradiance I) and perfectly distributed among all subcells. In Equation (2), the total losses in voltage increase by a factor of $N-1$, while the current density counters the effect by a factor of N. Its effect on the efficiency is shown in **Figure 5**. With the increasing number of subcells, the loss in efficiency saturates, as Equation (2) becomes independent of N when N approaches infinity

$$\Delta\eta|_{N\to\infty} = \Delta V_{TRJ} \cdot J_{ph-tot} \cdot FF/I \tag{3}$$

Such loss in efficiency equals 0.380% absolute considering the record $J_{ph\text{-}tot}$ = 32.9 mA cm^{-2} and the previously defined ΔV_{TRJ} and FF. In effect, with a finite number of subcells, the $\Delta\eta$ generally worsens with the increased number of subcells. As a consequence, the efficiency advantage of multijunction cells with more subcells is narrowed by the deteriorative effect of TRJs.

6. Filtered Illumination

From the optical perspective, the top subcell(s) in a multijunction solar cell acts as an optical filter which absorbs a part of the incident spectrum and reduces the irradiance arriving at the bottom subcell(s). Because the component subcells may receive illumination of a lower level when compared with their single-junction counterparts under the same incident solar spectrum, their photovoltaic performance could be quite different from the single-junction.

In particular, the V_{OC} of a solar cell is dependent on the illumination level as

$$V_{OC} = \frac{nkT}{e}\ln\frac{J_{ph}}{J_0} \tag{4}$$

where k and T are the Boltzmann constant and absolute temperature, respectively. At a given temperature, with a certain ideality factor n and dark saturation current density J_0 of the solar cell, the V_{OC} increases with the photocurrent density J_{ph} which is directly affected by the incident irradiance. Consequently, at two different illumination levels, the difference in V_{OC} of a solar cell is correlated to the ratio between the J_{ph}'s

$$\Delta V_{OC} = V'_{OC} - V_{OC} = \frac{nkT}{e}\ln\frac{J'_{ph}}{J_{ph}} \tag{5}$$

where [V_{OC}, J_{ph}] and [V'_{OC}, J'_{ph}] are two pairs of parameters under different illumination levels. For instance, assuming at T = 298.15 K, a nc-Si:H cell which has an ideality factor of 1.5, V_{OC} of 0.550 V and J_{ph} of 26.0 mA cm^{-2} under AM1.5G spectrum, if the J_{ph} is reduced to one fourth of its reference value due to the filtered illumination, then Equation (5) suggests a ΔV_{OC} of −53.43 mV and thus a V'_{OC} of 0.497 V under the filtered condition.

Equation (5) was applied to estimate the influence of filtered illumination on the performance of the studied multijunction structures. In the calculation, the ideality factor of all subcells was simplistically predetermined at a universal value of 1.5, and the reference parameters [V_{OC}, J_{ph}] were taken from Table 2. The result is shown in Table 5. Unlike the effect of TRJs, the loss in V_{OC} due to filtered illumination is not linear and it increases drastically with the number of subcells. The distribution of photocurrent to more subcells means less photocurrent generated in each subcell and greater deviation from the AM1.5G-reference performance of the single-junction counterparts. Equation (6) estimates how the filtered illumination affects the efficiency with increasing number of subcells

$$\Delta\eta = \frac{nkT\cdot FF}{eI}\frac{J_{ph-tot}}{N}\ln\frac{1}{N!} \tag{6}$$

It assumes the ideal device structure in which the J_{ph} of the Nth subcell is $1/N$ of the J_{ph} in the respective single-junction cell under AM1.5G spectrum. Such estimation of efficiency losses is illustrated in **Figure 6**. Both Table 5 and Figure 6 show that the difference in efficiency caused by filtered illumination clearly increases with the number of subcells. The considerable impact of filtered illumination limits the benefit of making multijunction solar cells comprising a large number of subcells.

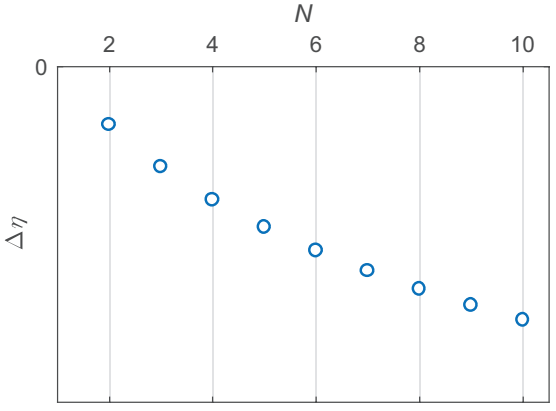

Figure 6. The loss in efficiency $\Delta\eta$ caused by the filtered illumination in multijunction solar cells increases with the number of subcells N, derived by Equation (6).

When the effects of TRJs and filtered illumination are both considered, the realistic photovoltaic performance of the multijunction solar cells further deviates from the optimistic estimation. As shown in Table 5, without these voltage losses, the difference in efficiency is 0.91% between D and TG, and 0.46% between TG and QG. Such efficiency improvement is reduced to merely 0.68% and 0.20%, respectively, when both losses are included. Even though the exact performance of these structures still depends on the light-trapping scheme (J_{SC}) and other device optimization (*FF*), the trend is revealed that there is an optimal number of subcells and the addition of subcells does not guarantee further improvement.

7. Thickness Limitations

The electronic transport properties of the materials can pose restrictions on the device structure, particularly on the thickness of the absorber layers. While thick absorber layers are desired for the optical absorption, thin layers are required to facilitate the carrier collection. In previous optical analyses, only the thickness of the bottommost nc-Si:H absorber layer was restricted at 3500 nm. The rest of the absorber layers were unconstrained to find the current-matching condition. The resultant structures are not always realistic. The top panel of **Table 6** shows the absorber thicknesses in the device structures of which the optical response is presented in Figure 2. The thicknesses of the (N)a-Si:H layers in structure D, QS, and QG, and of the a-SiGe$_x$:H layers in structure TG and QG are too thick to be electrically favorable. Especially, the electrical performance of a-SiGe$_x$:H (sub)cells deteriorates sharply with the increase in absorber thickness. It renders these certain configurations less practical for application.

Two adjustments were therefore deployed to improve the realistic performance estimation of the studied multijunction solar cells. First, the thickness of the a-SiGe$_x$:H layer in structure TG and QG was fixed at 250 nm, a reasonable value for providing decent electrical performance. Second, an 100 nm thick silicon oxide intermediate reflector (SOIR)[36,41] was inserted in the revised structure TG and QG behind the a-SiGe$_x$:H subcell, as well as in structure D and QS behind the (N)a-Si:H subcell, to compensate the reduced absorption in the thinner absorber layers. The result of the adjusted simulations is summarized in the bottom panel of Table 6. Without an intentional intermediate reflector, the constrained structures TG ltd. and QG ltd. severely suffer from the weak optical absorption, generating 1.41 and 2.77 mA cm^{-2} less total J_{ph} than their counterparts, respectively. The application of SOIR helps to bring the J_{ph} in the constrained TG back to a level comparable to the reference. A similar outcome is observed in the structure D and QS with SOIR, that the thicknesses of (N)a-Si:H are almost halved while the total J_{ph} only decreases by 0.44 and 0.64 mA cm^{-2}, respectively. On the other hand, the constrained QG cannot provide satisfactory J_{ph} even with SOIR. The limitation lies in the a-SiGe$_x$:H subcell that the required absorption is more than what it can realistically provide. It is true that the absoption spectrum of a-SiGe$_x$:H can be extended to longer wavelengths by incorporating more Ge atoms in the material, but the material with more Ge is more defective that the feasible thickness will be further limited. Therefore, with the analyses of optical and electrical losses as well as the thickness limitation from the materials, the constrained structures reported in Table 6 provide a more realistic estimation of what can be achieved with these multijunction structures. It is noteworthy that the estimated efficiencies of the structures D, TG and QG with SOIR presented in Table 6 align very well with the record initial efficiencies of the similar multijunction structures reported in literature,[12,14,28] when the difference in *FF* is taken into account.

Table 6. The thicknesses of the absorber layers in the studied multijunction structures, and the corresponding performance. t_1 means the absorber thickness of the first subcell from the surface of light incidence, etc. t_{tot} is the total thickness of all absorber layers. The values in bold indicate the thickness which was fixed in the current-matching algorithm of the simulations. The calculation of efficiency has included the influence of voltage losses.

Structure	t_1 [nm]	t_2 [nm]	t_3 [nm]	t_4 [nm]	t_{tot} [μm]	$J_{ph\text{-}tot}$ [mA cm^{-2}]	η [%]
D	549	**3500**	–	–	4.05	28.92	15.71
TS	196	2085	**3500**	–	5.78	29.41	15.28
TG	157	383	**3500**	–	4.04	28.45	16.39
QS	70.7	710	2812	**3500**	7.09	29.56	16.20
QG	61.1	531	817	**3500**	4.91	28.14	16.59
D w/SOIR	285	**3500**	–	–	3.79	28.48	15.46
TG ltd.	128	**250**	1951	–	2.33	27.04	15.53
TG ltd. w/SOIR	150	**250**	3212	–	3.61	28.18	16.22
QS w/SOIR	64.7	332	2642	**3500**	6.54	28.92	15.83
QG ltd.	45.8	281	**250**	1125	1.70	25.37	14.88
QG ltd. w/SOIR	48.7	315	**250**	1330	1.94	25.97	15.25

8. Optimal Number of Subcells

The preceding sections reveal the influence of different loss mechanisms on the performance of multijunction thin-film silicon solar cells. The assessments demonstrate how the benefit of multijunction cells can be compromised by several losses. On the other hand, the presented efficiencies are not meant to indicate the efficiency limit of this photovoltaic technology. The optical analyses thus the estimation of J_{SC} were based on the simulations on a certain type of light-trapping structure, which is the MST. The capability of a light-trapping structure is sometimes assessed by the achievable J_{SC} of the single-junction nc-Si:H cell on such structure. In this respect, the honeycomb structure deployed in n–i–p configuration holds the record of 32.9 mA cm^{-2}.[33] Our optical analyses might be extrapolated to the application of the honeycomb structure by assuming the same differences in total J_{ph} between the single-junction and multijunction cells. For example, the total J_{ph} on the MST obtained in simulations is 28.86 and 25.97 mA cm^{-2} for the single-junction S and the revised structure QG, respectively. Then, from 32.9 mA cm^{-2} in the single-junction, the total J_{ph} in the revised QG on the honeycomb structure was speculated at 30.01 mA cm^{-2}. By doing so, the implied efficiencies of structures D, TS, TG, QS, and QG (all with SOIR and with

thickness limitation considered) on the honeycomb structure were extrapolated to 17.78%, 17.51%, 18.67%, 18.17%, and 17.75%, respectively, with all the voltage losses considered. The estimated efficiencies are higher with the better light-trapping structure, yet the general trend remains the same. Among the studied structures of thin-film silicon solar cells, structure TG, the triple-junction cell with a-$SiGe_x$:H subcell, is the most promising in terms of initial efficiency.

The optimal number of subcells is decided by the balance between the gains and losses occurred in the multijunction solar cells. The gains are typically identified as the increase in output voltage offered by the absorber materials with wider bandgap. Such gains are greater when the solar cells feature a higher ratio of eV_{OC}/E_g,[42] where E_g is the bandgap. As it was demonstrated, the losses grow mainly with the number of subcells, not directly with the amount of gains. For thin-film silicon solar cells, the optimum happens to be the triple-junction configuration. Beyond triple-junction, the additional losses become comparable to or even more than the gain in voltage.

The loss mechanisms investigated in this work are common to all two-terminal multijunction solar cells. Therefore, similar analyses can be conducted for other photovoltaic material systems. However, the quantitative results cannot be directly transferred between different technologies, since the extent of influence of each loss mechanism is decided by the specific materials and device structure. For example, the degree of optical loss will depend on the optical constants of the materials.

The optimum number of junctions may be different for different technologies. For a photovoltaic technology with higher eV_{OC}/E_g, such as the III-V solar cells, the significant gains leave more room for efficiency improvement by adding subcells before the losses neutralize the additional gains. This should be regarded as an important criterion when one considers developing multijunction solar cells comprising a large number of subcells.

9. Variations in Photocurrent Generation

When multijunction solar cells generate more power than the single-junction cell does, they also shift the operation regime to that of higher voltages and lower current densities because the component subcells are connected in series. As the current density becomes lower along such regime transition induced by increasing the number of subcells, the power conversion efficiency of the solar cells becomes more and more sensitive to any changes in the current density.

To illustrate, we can consider the structures and parameters presented in Table 3, where the photocurrents are perfectly matched between the subcells and the total J_{ph} are all the same at 32.9 mA cm^{-2}. If a certain variation reduces the photocurrent in the single-junction cell by 1.0 mA cm^{-2}, the J_{SC} goes down by 3.0%. In contrast, if a similar variation decreases the photocurrent in one of the subcells of a quadruple-junction cell by 1.0 mA cm^{-2}, then the J_{SC} is also reduced by roughly 1.0 mA cm^{-2}, which accounts for a relative reduction of 12.2%, considerably more than that in the single-junction. Apparently, the solar cell with a larger number of subcells is more susceptible to such variations.

The consequences of the susceptibility of multijunction solar cells are twofold. In the first place, it requires very high standards for the accuracy, uniformity, and reproducibility of the fabrication processes of the multijunction cells, alongside the delicate engineering needed for realizing a well current-matched device. A difference in thickness of 10 nm in the top part of a cell can lead to a difference in photocurrent of more than 0.5 mA cm^{-2}, which is significant in a multijunction cell with many subcells. Therefore, any temporal or spatial inconsistency in the fabrication processes can result in a considerable discrepancy in the device performance. Beside the manufacturing, it also makes the development of high-efficiency multijunction solar cells more difficult from the beginning.

Another problem of the susceptibility is in the terrestrial application. The solar spectrum incident at a certain location is subject to daily and seasonal variations. Not only the overall intensity but also the spectral distribution of the solar irradiation changes over time due to the influence of the celestial position, the atmosphere, and the weather. Because of the aforementioned susceptibility, the spectral variations of sunlight can strongly impact the performance of multijunction solar cells.

As a demonstration, the photocurrents of the studied structures in the top panel of Table 6 were derived under different solar spectra. The transmission model SPCTRAL2[43] was used to simulate the solar spectra in different seasons, namely the summer (21 June), autumn (18 October) and winter (21 December) at noon of the given days. The incident surface was defined by coordinates of 52.00°N 4.37°E (Delft, The Netherlands), tilt angle of 37.0°, and azimuth angle of 180° (South). Together with the AM1.5G spectrum, the simulated spectra are depicted in **Figure 7**a. With each solar spectrum, integrating the simulated spectral response of the multijunction structures in Figure 2 by Equation (1) gives the J_{ph} of each subcell. **Figure 8**a–c shows the resulted J_{ph} for three multijunction structures. Since their distribution of optical absorption was optimized for the AM1.5G spectrum, the photocurrents among the subcells are uniform under AM1.5G but have discrepancies under the seasonal spectra. To quantify the excess J_{ph} which cannot be utilized due to the series connection between the subcells, the ratio of photocurrent utilization (U) is defined as the ratio of the collectible J_{ph} to the total generated J_{ph}

$$U = \frac{NJ_{ph-min}}{\sum_{i=1}^{N} J_{ph_i}} \tag{7}$$

where J_{phi} is the J_{ph} of the ith subcell and $J_{ph\text{-}min}$ is the lowest one among all subcells in a multijunction cell. In Figure 8, naturally, the ratio of photocurrent utilization is effectively 100% under the AM1.5G spectrum.

In this example, among the seasonal solar spectra, the highest U is observed in autumn for all structures, while the lowest is in winter, as shown in Figure 8d. This can be explained by the similarity/difference between the seasonal spectrum and the AM1.5G spectrum, for which the multijunction structures were optimized. The degree of similarity is clearly illustrated in Figure 7b, in which the spectral photon flux density Φ of the seasonal spectrum is normalized according to the respective value in AM1.5G spectrum $\Phi_{AM1.5G}$. Ideally, if a spectrum

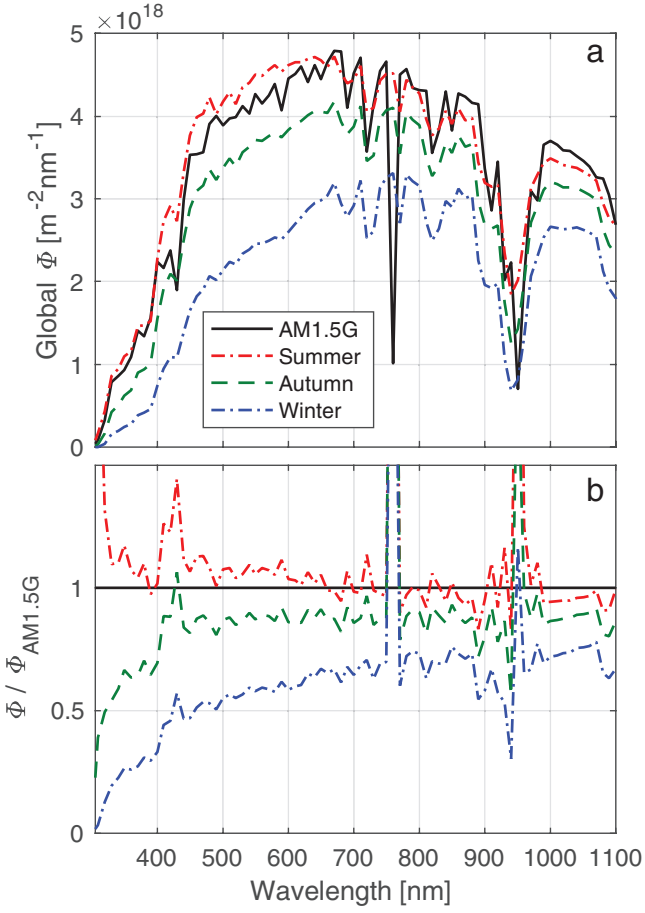

Figure 7. a) Spectral photon flux density Φ of the solar spectra received at a certain location in Delft in different seasons, simulated by the model SPCTRAL2. The AM1.5G spectrum is also plotted as reference. b) The seasonal spectra normalized to the AM1.5G spectrum, to visualize whether a spectrum has a similar spectral profile to AM1.5G.

exhibits a horizontal line in this figure, such spectrum has the same spectral profile as the AM1.5G spectrum, then an AM1.5G-optimized multijunction cell will operate in the current-matched condition under this spectrum. In Figure 7b, the autumn spectrum shows mostly horizontal in this wavelength range, agrees with the highest U in the studied structures. In contrast, the summer spectrum is more intense in the short wavelengths while the winter one is more intense in the long wavelengths, both result in uneven distribution of J_{ph} and thus lower U. Therefore, it is evident that a multijunction cell optimized for a certain solar spectrum will result in current mismatch thus incomplete photocurrent utilization under a different spectrum. It can also be observed in Figure 8d that the losses in U become larger with the increased number of subcells. In addition, the negative impact on the power conversion efficiency is further aggravated with the number of subcells because the influence of the lost J_{ph} is enlarged by the higher output voltage of the multijunction cells with a large number of subcells. As a result, the more subcells a multijunction solar cell has, the greater its photovoltaic performance suffers from changes in the solar spectrum.

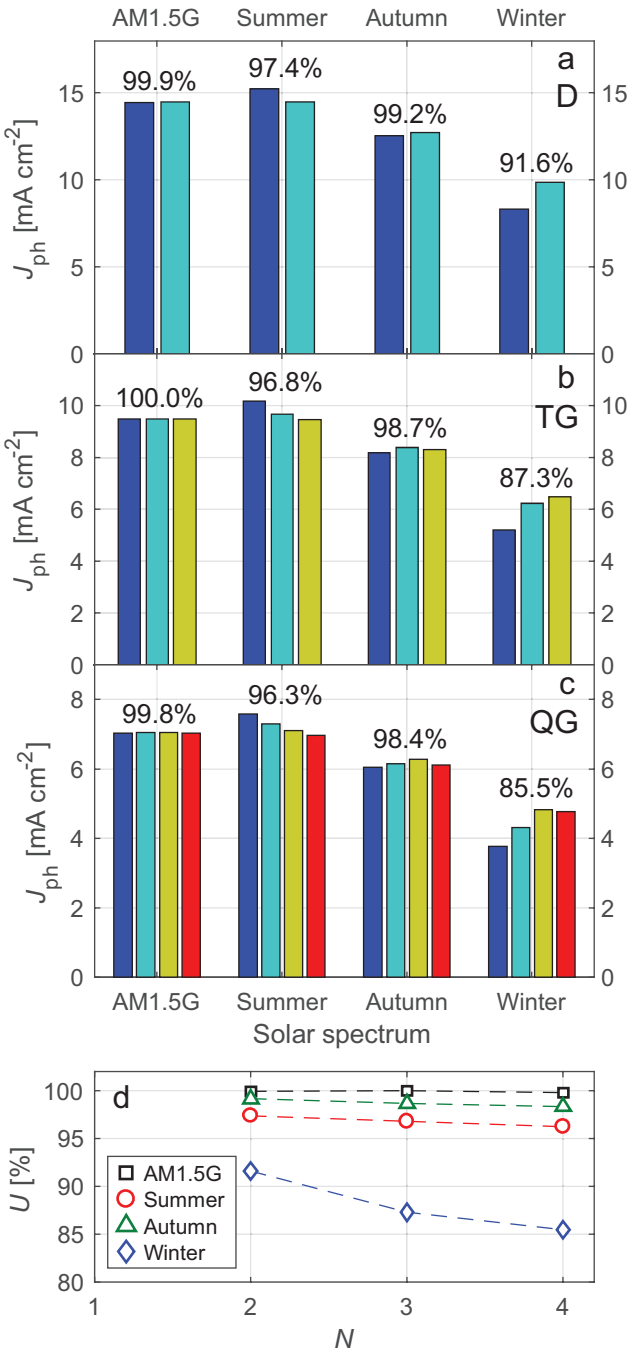

Figure 8. a–c) The distribution of J_{ph} generated in the studied multijunction structures under different solar spectra, and d) the corresponding ratio of photocurrent utilization (U). The percentages indicated in panels (a)–(c) are the respective ratio U.

The analysis with the simulated solar spectra decidedly demonstrates how the spectral variation can deteriorate the photocurrent utilization of multijunction solar cells. It should be noted that the spectra shown in Figure 7a only take into account the solar position in relation to the location of the incident surface and emphasize the difference between the seasons. Besides, the solar spectrum is subjected to many other

factors such as clouds, albedo, air composition, etc. All of these factors can affect the photocurrent utilization in multijunction solar cells, although the precise simulation of solar spectrum under different detailed circumstances is out of the scope of this study.

10. Conclusions

Is making multijunction solar cells with a large number of subcells beneficial? Using the information from thin-film silicon photovoltaics, several loss mechanisms inherent in multijunction cells have been discussed. Optically, both the parasitic absorption and reflection losses slightly increase with the number of subcells. The parasitic absorption is decided by the transparency of the supporting materials and the optical utilization of the topmost subcell. The reflection losses are raised whenever a new subcell is encountered by the light. Electrically, tunnel recombination junctions induce a drop in the output voltage, but the effect on the power conversion efficiency saturates at a large number of subcells. The influence of the filtered illumination received by the subcells appears to be more detrimental since the increase of voltage loss with the number of subcells is faster than a linear growth. Overall, the efficiency potential of multijunction solar cells is decided by the losses counteracting the gains from the added subcells, which is largely determined by the ratio of the output voltage to the bandgap of the absorber materials. In generic terrestrial (i.e., nonconcentration, nontracking, and nondesert-climate) applications, multijunction solar cells could be less appealing because the efficiency suffers from the daily and seasonal changes in the solar spectrum.

Acknowledgements

The authors thank Dr. Rudi Santbergen for the discussion on optical simulations, and thank Dr. Alexander Mellor for carefully reviewing the language of the manuscript. This work was supported by the Foundation for Fundamental Research on Matter (FOM), which is part of the Netherlands Organization for Scientific Research (NWO).

Conflict of Interest

The authors declare no conflict of interest.

Keywords

loss analysis, multijunction solar cells, photovoltaic cells, thin-film silicon, two-terminal monolithic cells

Received: May 23, 2017
Revised: August 18, 2017
Published online: September 22, 2017

[1] S. Rühle, *Sol. Energy* **2016**, *130*, 139.
[2] W. Shockley, H. J. Queisser, *J. Appl. Phys.* **1961**, *32*, 510.
[3] A. De Vos, *J. Phys. D: Appl. Phys.* **1980**, *13*, 839.
[4] H. Cotal, C. Fetzer, J. Boisvert, G. Kinsey, R. King, P. Hebert, H. Yoon, N. Karam, *Energy Environ. Sci.* **2009**, *2*, 174.
[5] D. J. Friedman, *Curr. Opin. Solid State Mater. Sci.* **2010**, *14*, 131.
[6] J. Ohlmann, J. F. M. Sanchez, D. Lackner, P. Förster, M. Steiner, A. Fallisch, F. Dimroth, in *AIP Conf. Proc., American Institute of Physics, Melville, NY* **2016**, p. 80004.
[7] Sharp Develops Concentrator Solar Cell with World's Highest Conversion Efficiency of 44.4%, http://www.sharp-world.com/corporate/news/130614.html, accessed September 2017.
[8] F. Dimroth, T. N. D. Tibbits, M. Niemeyer, F. Predan, P. Beutel, C. Karcher, E. Oliva, G. Siefer, D. Lackner, P. Fus-Kailuweit, A. W. Bett, R. Krause, C. Drazek, E. Guiot, J. Wasselin, A. Tauzin, T. Signamarcheix, *IEEE J. Photovoltaics* **2016**, *6*, 343.
[9] M. A. Green, Y. Hishikawa, W. Warta, E. D. Dunlop, D. H. Levi, J. Hohl-Ebinger, A. W. H. Ho-Baillie, *Prog. Photovoltaics Res. Appl.* **2017**, *25*, 668.
[10] H. Sai, K. Maejima, T. Matsui, T. Koida, M. Kondo, S. Nakao, Y. Takeuchi, H. Katayama, I. Yoshida, *Jpn. J. Appl. Phys.* **2015**, *54*, 08KB05.
[11] T. Matsui, A. Bidiville, K. Maejima, H. Sai, T. Koida, T. Suezaki, M. Matsumoto, K. Saito, I. Yoshida, M. Kondo, *Appl. Phys. Lett.* **2015**, *106*, 53901.
[12] H. Tan, E. Moulin, F. T. Si, J.-W. Schüttauf, M. Stuckelberger, O. Isabella, F.-J. Haug, C. Ballif, M. Zeman, A. H. M. Smets, *Prog. Photovoltaics Res. Appl.* **2015**, *23*, 949.
[13] H. Sai, T. Matsui, K. Matsubara, *Appl. Phys. Lett.* **2016**, *109*, 183506.
[14] B. Yan, G. Yue, L. Sivec, J. Yang, S. Guha, C.-S. Jiang, *Appl. Phys. Lett.* **2011**, *99*, 113512.
[15] D. J. You, S. H. Kim, H. Lee, J.-W. Chung, S.-T. Hwang, Y. H. Heo, S. Lee, H.-M. Lee, *Prog. Photovoltaics Res. Appl.* **2015**, *23*, 973.
[16] X. Multone, L. Fesquet, D. Borrello, D. Romang, G. Choong, E. Vallat-Sauvain, M. Charrière, A. Billet, J.-F. Boucher, J. Steinhauser, J.-B. Orhan, R. Monnard, J.-P. Cardoso, G. Charitat, B. Dehbozorgi, N. Guillot, G. Monteduro, M. Marmelo, R. Semenzi, S. Benagli, J. Meier, *Sol. Energy Mater. Sol. Cells* **2015**, *140*, 388.
[17] M. Stuckelberger, R. Biron, N. Wyrsch, F.-J. Haug, C. Ballif, *Renewable Sustainable Energy Rev.* **2017**, *76*, 1497.
[18] T. Ameri, G. Dennler, C. Lungenschmied, C. J. Brabec, D. Waller, R. Gaudiana, C. J. Brabec, A. J. Heeger, P. W. M. Blom, M. Koch, K. Leo, M. Pfeiffer, H. Hoppe, D. Meissner, N. S. Sariciftci, I. Riedel, V. Dyakonov, J. Parisi, *Energy Environ. Sci.* **2009**, *2*, 347.
[19] T. Ameri, N. Li, C. J. Brabec, *Energy Environ. Sci.* **2013**, *6*, 2390.
[20] J. You, L. Dou, Z. Hong, G. Li, Y. Yang, *Prog. Polym. Sci.* **2013**, *38*, 1909.
[21] J. P. Mailoa, C. D. Bailie, E. C. Johlin, E. T. Hoke, A. J. Akey, W. H. Nguyen, M. D. McGehee, T. Buonassisi, *Appl. Phys. Lett.* **2015**, *106*, 121105.
[22] S. Albrecht, M. Saliba, J. P. Correa Baena, F. Lang, L. Kegelmann, M. Mews, L. Steier, A. Abate, J. Rappich, L. Korte, R. Schlatmann, M. K. Nazeeruddin, A. Hagfeldt, M. Grätzel, B. Rech, *Energy Environ. Sci.* **2016**, *9*, 81.
[23] J. Werner, C.-H. Weng, A. Walter, L. Fesquet, J. P. Seif, S. De Wolf, B. Niesen, C. Ballif, *J. Phys. Chem. Lett.* **2016**, *7*, 161.
[24] K. A. Bush, A. F. Palmstrom, Z. J. Yu, M. Boccard, R. Cheacharoen, J. P. Mailoa, D. P. McMeekin, R. L. Z. Hoye, C. D. Bailie, T. Leijtens, I. M. Peters, M. C. Minichetti, N. Rolston, R. Prasanna, S. Sofia, D. Harwood, W. Ma, F. Moghadam, H. J. Snaith, T. Buonassisi, Z. C. Holman, S. F. Bent, M. D. McGehee, *Nat. Energy* **2017**, *2*, 17009.
[25] T. Todorov, T. Gershon, O. Gunawan, Y. S. Lee, C. Sturdevant, L.-Y. Chang, S. Guha, *Adv. Energy Mater.* **2015**, *5*, 1500799.
[26] H. Tan, A. Furlan, W. Li, K. Arapov, R. Santbergen, M. M. Wienk, M. Zeman, A. H. M. Smets, R. A. J. Janssen, *Adv. Mater.* **2016**, *28*, 2170.
[27] P. T. Chiu, D. Law, R. L. Woo, S. B. Singer, D. Bhusari, W. D. Hong, A. Zakaria, J. Boisvert, S. Mesropian, R. R. King, N. H. Karam, in

2014 IEEE 40th Photovoltaic Specialist Conf., IEEE, Piscataway, NJ, **2014**, pp. 0011–0013.
[28] B. Liu, L. Bai, T. Li, C. Wei, B. Li, Q. Huang, D. Zhang, G. Wang, Y. Zhao, X. Zhang, *Energy Environ. Sci.* **2017**, *10*, 1134.
[29] F. T. Si, D. Y. Kim, R. Santbergen, H. Tan, R. A. C. M. M. van Swaaij, A. H. M. Smets, O. Isabella, M. Zeman, *Appl. Phys. Lett.* **2014**, *105*, 63902.
[30] F. T. Si, O. Isabella, H. Tan, M. Zeman, *Sol. RRL* **2017**, *1*, 1700036.
[31] J.-W. Schüttauf, B. Niesen, L. Löfgren, M. Bonnet-Eymard, M. Stuckelberger, S. Hänni, M. Boccard, G. Bugnon, M. Despeisse, F.-J. Haug, F. Meillaud, C. Ballif, *Sol. Energy Mater. Sol. Cells* **2015**, *133*, 163.
[32] T. Matsui, K. Maejima, A. Bidiville, H. Sai, T. Koida, T. Suezaki, M. Matsumoto, K. Saito, I. Yoshida, M. Kondo, *Jpn. J. Appl. Phys.* **2015**, *54*, 08KB10.
[33] H. Sai, T. Matsui, T. Koida, K. Matsubara, M. Kondo, S. Sugiyama, H. Katayama, Y. Takeuchi, I. Yoshida, *Appl. Phys. Lett.* **2015**, *106*, 213902.
[34] R. Santbergen, T. Meguro, T. Suezaki, G. Koizumi, K. Yamamoto, M. Zeman, *IEEE J. Photovoltaics* **2017**, *7*, 919.
[35] O. Isabella, F. Moll, J. Krč, M. Zeman, *Phys. Status Solidi A* **2010**, *207*, 642.
[36] M. Boccard, C. Battaglia, S. Hänni, K. Söderström, J. Escarré, S. Nicolay, F. Meillaud, M. Despeisse, C. Ballif, *Nano Lett.* **2012**, *12*, 1344.
[37] M. Zeman, O. Isabella, S. Solntsev, K. Jäger, *Sol. Energy Mater. Sol. Cells* **2013**, *119*, 94.
[38] K. Jäger, M. Fischer, R. A. C. M. M. van Swaaij, M. Zeman, *J. Appl. Phys.* **2012**, *111*, 83108.
[39] A. N. Corpus-Mendoza, M. M. De Souza, F. Hamelmann, *J. Appl. Phys.* **2013**, *114*, 184505.
[40] B. Liu, L. Bai, Z. Chen, X. Zhang, D. Zhang, J. Ni, Q. Huang, C. Wei, J. Sun, X. Chen, H. Ren, G. Hou, G. Wang, Y. Zhao, *Prog. Photovoltaics Res. Appl.* **2015**, *23*, 1313.
[41] P. Buehlmann, J. Bailat, D. Dominé, A. Billet, F. Meillaud, A. Feltrin, C. Ballif, *Appl. Phys. Lett.* **2007**, *91*, 143505.
[42] A. Polman, M. Knight, E. C. Garnett, B. Ehrler, W. C. Sinke, *Science* **2016**, *352*, aad4424.
[43] R. E. Bird, C. Riordan, R. E. Bird, C. Riordan, *J. Clim. Appl. Meteorol.* **1986**, *25*, 87.

